Iranian Journal of Materials Science and Engineering, Vol. 19, Number 4, December 2022
RESEARCH PAPER

Comparative Analysis on Reinforcement of Potential Additives in WOKA Cermet HVOF Coating Subjected to Slurry Erosion in Ash Conditions

Jasganpreet Singh[1,*], Rana Gill[1,2], Satish Kumar[3], S. K. Mohapatra[4]

* *ijashanpreet@gmail.com*

[1] University Center for Research & Development, Chandigarh University, Mohali 140413, India
[2] Department of Electronics and Communication Engineering, Chandigarh University, Mohali 140413, Punjab, India
[3] Department of Mechanical Engineering, National Institute of Technology, Jamshedpur 831014, Jharkhand, India
[4] Mechanical Engineering Department, Thapar Institute of Engineering and Technology, Patiala 147004, Punjab, India

Received: May 2022 **Revised: October 2022** **Accepted: November 2022**
DOI: 10.22068/ijmse.2834

Abstract: *In this paper, an investigation was carried out to test the suitability of potential additive materials in WOKA 3533 (WC-10Co$_4$Cr) cermet HVOF coating subjected to slurry erosion in ash conditions. The additives namely molybdenum carbide, yttrium oxide, and zirconium oxide were added in equal percentages (3 wt.%) in WOKA cermet powder. High-velocity oxy-fuel (HVOF) spraying was performed to develop the additive-based WOKA cermet coatings. The slurry erosion in ash conditions was tested using the pot tester. Microstructural and mechanical properties of traditional and additive-based WOKA cermet coatings were also tested in the present study; for example, microstructure, crystalline phases of as-sprayed coatings, and microhardness. Results present a comparison of surface erosion wear of different cermet coatings. It was found that the yttrium oxide was a suitable additive for the WOKA cermet coatings than the molybdenum carbide. However, zirconium oxide is unsuitable for WOKA cermet coatings in erosion wear applications.*

Keywords: *Slurry erosion, HVOF coating, cermet, slurry pump, ash transportation.*

1. INTRODUCTION

Solid particle slurry erosion is a problematic issue that is associated with deterioration caused by the flow of different slurries [1]. Slurry erosion behaves dominant at accelerated conditions therefore, it shortens the life of equipment [2]. Slurry erosion is found most common in mining, chemical industries, and thermal power plants. Pump casings/impellers, nozzles, reducers/expanders, valves, flanges, tubes/pipelines, tees/elbows, etc. are the major worn-out components in ash disposal as well as other slurry conveying systems [3–6] Most dangerous accelerated conditions are observed at the pump casing and impeller. Usually, centrifugal slurry pumps are used to transport the different slurries in the industrial sector. Also, the erosion wear due to gas-solid is relatively well understandable than solid-liquid erosion.

The slurry erosion of materials depends on the variety of parameters that comprises properties of flowing medium and material, and process parameters [7, 8]. A small variation in any of the parameters affects the erosion wear process. Hence, the present study is also aimed to investigate the physical and chemical properties of erodent materials.

The life of the pump and its components can be improved either by changing the design of the components or by changing the material or/and surface properties [9–13]. The high-velocity oxy-fuel (HVOF) spraying process is the most versatile coating deposition process among the different processes [7, 9, 21–25, 11, 14–20]. HVOF process can be used for pure metals as well as ceramics/cermet [26–28]. Generally, commercially available WC–Co, Al, and Ni-Cr-based coatings were used to reduce the slurry erosion in pump materials [13, 29–31]. Although numerous researchers have employed WC-based coatings to enhance the slurry erosion resistance to stainless steels and found these coatings effective in use. WOKA powder coating is extensively utilized in many industrial applications [32–34]. Regarding WC-Co-Cr spray-deposited coatings, a lot of literature is accessible.

An overview is carried out to provide the current scenario about erosion wear of WC-based coatings. Investigators have made efforts to find

[DOI: 10.22068/ijmse.2834]

the erosion wear by carrying out lab scale and pilot plant test loops. In a novel experimental approach, Wheeler and Wood [32] measured the wear on an AISI 1020 steel surface coated with WOKA powder (10% Co and 4% Cr) powder. To study the slurry erosion, they conducted tests on WOKA coating and steel using sand slurry utilizing the jet erosion facility. The erosion resistance of the D-gun coated specimen was found to be two times higher than the slurry erosion resistance of the diatec HVOF-WOKA (10% Co and 4% Cr) coating. Cho et al. [35] studied the morphology and performance of HVOF-deposited WC-Co coatings on carbon steel with the addition of Nano and micron powders. They performed coating using Nano (0.1–1 μm) and micron (1–40 μm) sized powders mixed to WC-Co by 12 and 88% (by wt.) respectively. They found that coating hardness is strongly dependent on spray parameters and powder size. For comparison, the Nano WC-Co has a hardness smaller than the micro WC-Co because Nano WC-Co decomposes into coarser compounds (coarse W_2C, W, and graphite) as compared to micro WC-Co. The evolution of undesirable carbon oxide gases in micro WC–Co coating was detected lower than in Nano WC–Co coating therefore it possesses lower porosity as compared to Nano WC–Co. Thakur et al. [36] reported that the slurry erosion characteristic of standard and modified WOKA (Nano WC added) sprayed surface utilizing a pot tester. They performed erosion wear testing with varying erodent sizes and slurry concentrations. Results showed that higher erosion resistance was observed at all testing parameters for fine WC in WOKA cermet coating in comparison to standard WOKA cermet coating. Vite-Torres et al. [37] investigated the AISI 420 stainless steel's ability to sustain erosion. To develop the slurry conditions, they utilized silicon carbide (angular) and spherical grit particles as erodent particles. Experiments were done using a jet impingement tester. Variations in particle size (400-420 μm), impact angle (30-90°), and speed erodent were done during the performed experiments. They found that shape of erodent impacts erosion wear rate. The elliptical shape of scars was noted at an impact angle of 30° wide and circular at 60°. They reported that erosion is most significant at impact angles of 30° or more, confirming that the material showed ductile behavior. Singh et al. [38] tested the erosion performance of WOKA cermet HVOF coatings subjected to silt slurry erosion. This study is carried forward for the fly and bottom ash slurry in the present investigation. The comprehensive literature survey represents that the HVOF surface modification technique is preferred to improve the slurry erosion resistance of pump materials. WOKA cermet coatings are found promising in slurry erosion applications however they can be improved by adding a small amount of ceramics. So, there is still a need to improve the WOKA coatings for withstanding long against ash slurry erosion conditions. The fulfillment of need will lead to the development of novel modified WOKA coatings. In the present study, various novel thermal spraying powders were used to improve slurry erosion resistance for the substrate materials. The HVOF process is highly preferable in the case of WOKA coating; therefore, chosen in the present study. The synergistic effect of the addition of additives with suitability in WOKA cermet coating is also explained in this paper.

2. EXPERIMENTAL PROCEDURE

2.1. Base Material

The workpiece of SS316L was used as a base material for the coating deposition as shown in Fig. 1. Test specimens have dimensions of 67.5 × 25.0 × 5.0 mm.

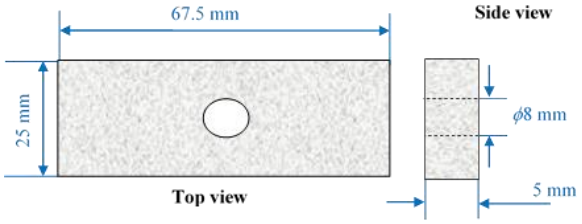

Fig. 1. Specimen used for coating deposition

2.2. Coating Powders and Deposition Technique

In the present study, ceramics and cermet are used to improve the erosion wear performance of pump materials. The additives namely molybdenum carbide, yttrium oxide, and zirconium oxide were added in equal percentages (3 wt. %) in WOKA 3533 (WC-10Co4Cr) cermet powder. WOKA (45±15 μm) and molybdenum carbide (60±15 μm) were bought from Parshwamani Metals, Mumbai (India). Yttrium oxide (30±15 μm) and zirconium oxide (10±5 μm) were bought from High Purity Laboratory Chemicals Private

[DOI: 10.22068/ijmse.2834]

Limited, Srigam (India). The surface morphology was carried out prior which is shown in Fig. 2. The blending of different powders was done by using Jar ball milling. The bearing balls used in the Jar mill are made of hardened steel and have a diameter of 2 cm. The newly built WOKA-molybdenum carbide, WOKA-yttrium oxide, and WOKA-zirconium oxide were designated as WOKA-M, WOKA-Y, and WOKA-Z, respectively.

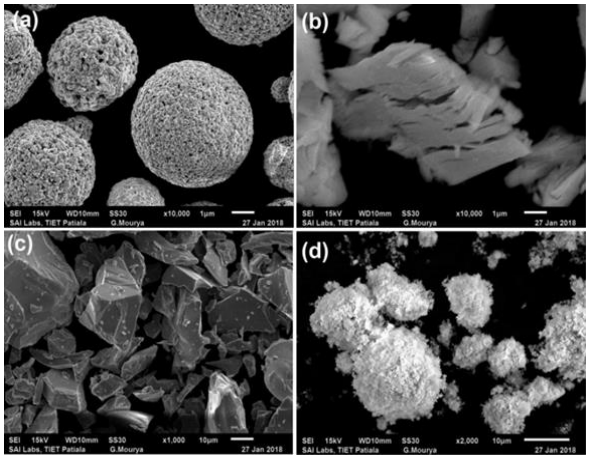

Fig. 2. Surface morphology of (a) WOKA, (b) Yttrium oxide, (c) Molybdenum carbide, and (d) Zirconium oxide powders

The coating deposition process proceeded following the grit-blasting process. Quartz was used for the grit blasting to provide an irregular pattern to the workpiece surface. For this process, a grit blasting unit (Abrablast Equipment Pvt. Ltd., Jodhpur, India) was employed.

This process guarantees adherence between the base material and the coating layer. High-velocity oxy-fuel (HVOF) spraying was performed to develop the traditional and additive-based WOKA cermet coatings. HVOF coatings were done using the MP-2100 coating facility assembled with the HP-2700 torch. HVOF facility was maintained at different optimized parameters as listed in Table 1.

2.3. Characterization Methodology

The microstructure was analyzed for the as-coated surface with the use of the scanning electron microscopy (SEM) technique. A Philips X'pert Diffractometer (Model: PW-1710, Philips, The Netherlands) was used to trace the X-ray diffractograms. The Vickers indentation technique was used to assess the microhardness of standard and modified WOKA coatings. The microhardness tester (Metatech: MVH-1, Pune, India) was used to do the measurement. The indentation load ranged from 500 to 1,000 grams throughout testing.

The surface roughness tester was assisted with the measurement of average roughness on the surface (Surftest roughness tester: SJ-400, Mitutoyo, USA). During the roughness experiments, the test area was taken as 0.00125 m.

2.4. Slurry Erosion Experiments

In this work, a pot tester was used to perform the slurry erosion experimentation. As per the ASTM G76–95 method [39], a jet tester is recommended for erosion experimentation for the gas-solid. On the other hand, the jet tester can't be used for the high concentration slurries i.e. >30 wt. %. Therefore, a pot tester is suitable equipment for slurry erosion experiments. Desale et al. (2006) suggested the use of a pot tester for the evaluation of slurry erosion in pumps and pipelines in case of solid-liquid flow. The pot tester was run at different speeds during the experimentation. The concentration of erodent materials was taken in the range of 30-60 wt. %.

The pot tester was run at different speeds lying in the range of 600-1500 rpm with an increment of 300 rpm. The pot tester was run at different speeds to produce different velocities. Slurry erosion testing time was taken in the range of 90 to 180 minutes. The experiments were conducted by preparing the fly ash (FA) and bottom ash (BA) slurries.

The slurry was prepared in different weight proportion percentages by utilizing the mixing motion of 300 rpm produced with the help of a magnetic stirrer. The prepared slurry was poured into the slurry vessel i.e. pot of tester. The water vessel was filled with freshwater to facilitate the cooling of the slurry vessel. The jackscrew was moved to adjust the height of the slurry vessel. Afterward, the spindle's speed was adjusted at a required level to produce the rotational speed of the workpiece. Over time, each worn-out workpiece was measured for the evaluation of weight loss (unit: g). The slurry erosion was calculated as weight loss (g)/area of the specimen (m^2).

[DOI: 10.22068/ijmse.2834]

Table 1. Parameters maintained throughout the HVOF coating

→ Parameters Powders↓	Spray parameters							
	Flow rate (SPLM)			Pressure (kg/cm^3)			Powder feed rate (g/min)	Spray distance (mm)
	Oxygen	Air	Fuel	Oxygen	Air	Fuel		
WOKA/ WOKA-M	260	640	60	10	6	7.5	30	150
WOKA-Z/ WOKA-Y	245	690	70	10	6	7.5	25	150

3. RESULTS AND DISCUSSION

3.1. Microstructure of Coatings

SEM micrographs of WOKA, WOKA-Y, WOKA-M, and WOKA-Z coatings are represented in Fig. 3. In Fig. 3(a), the splats, pores, and unburnt particles were evident on the as-HVOF sprayed WOKA coating. Partially melted areas were detected on the as-HVOF sprayed WOKA-Y surface, as illustrated in Fig. 3(b).

HVOF sprayed surface WOKA-M and WOKA-Z coatings show melted lamellae splats and pores, as observed in Fig. 3(c, d). Lamellae splats are usually developed in HVOF coating, as reported in previous studies [40].

3.2. XRD of As-sprayed Surface

X-ray diffractograms reveal the crystalline phase in WOKA coatings as shown in Figure 4. XRD results of larger peaks are summarized in Table 2. In Fig. 4(a), WOKA HVOF coating is composed of above mentioned crystalline phases however, the WC phase is brittle/fragile and expected to crack, crater, or fracture. The results are well pronounced in previous studies [41, 42].

3.3. Microhardness Analysis

The average microhardness of the WOKA is tabulated in Table 2. These results show good agreement with previous studies [4, 41, 42].

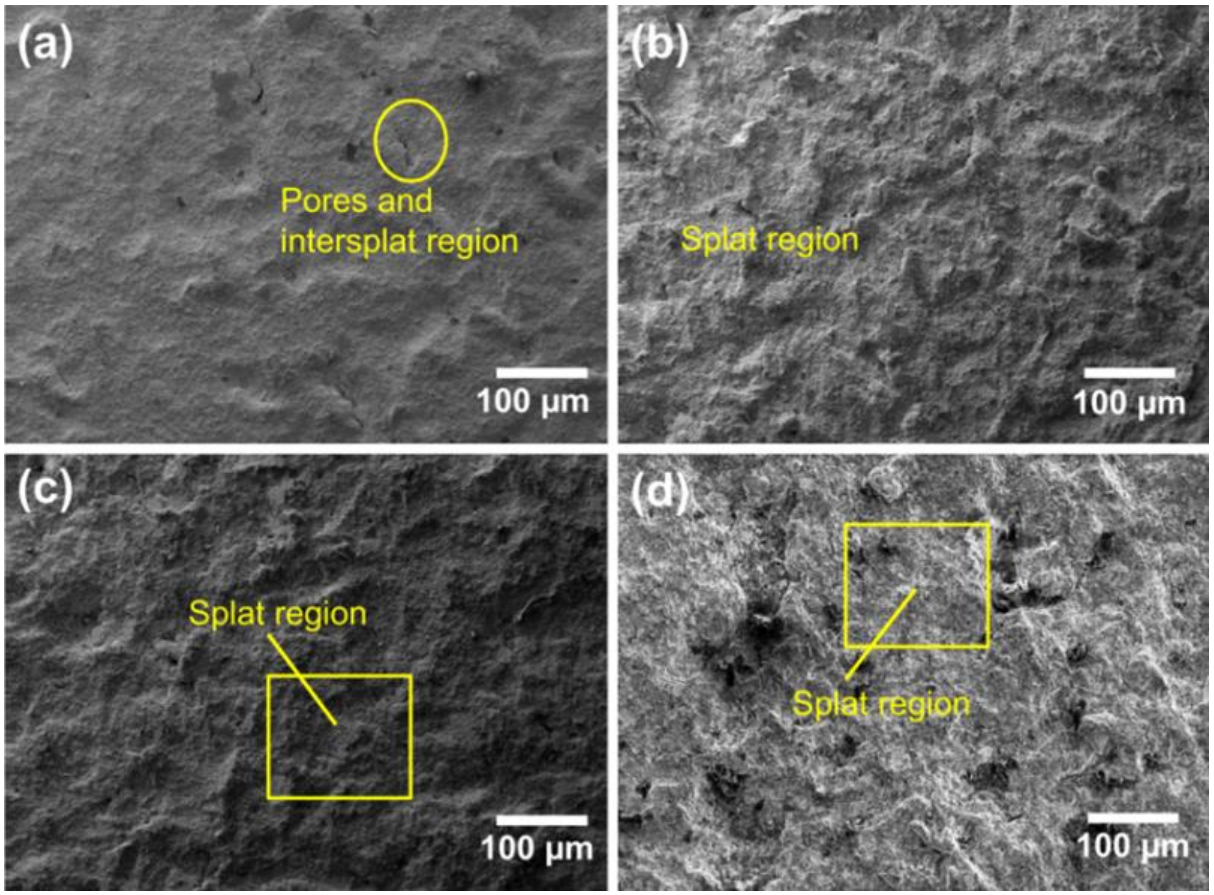

Fig. 3. SEM micrographs of (a) WOKA, (b) WOKA-Y, (c) WOKA-M, and (d) WOKA-Z coatings at a magnification of ×100

[DOI: 10.22068/ijmse.2834]

Table 2. Properties of HVOF coating

Property	WOKA	WOKA-Y	WOKA-M	WOKA-Z
Crystalline phases	WC, W_2C, $Cr_{26}C_6$, Cr_7C_3, and CoC	WC, Co_6W_6C, Cr_7C_3, and α-Y_2O_3	WC, W_2C, α-Mo_2C, $Cr_{26}C_6$, Cr_7C_3, and CoC	WC, W_2C, $Cr_{23}C_6$, Cr_3C_7, CoC, and α-ZrO_2
Microhardness (H.V.)	1156± 27	1164± 21	1123±18	1089±32

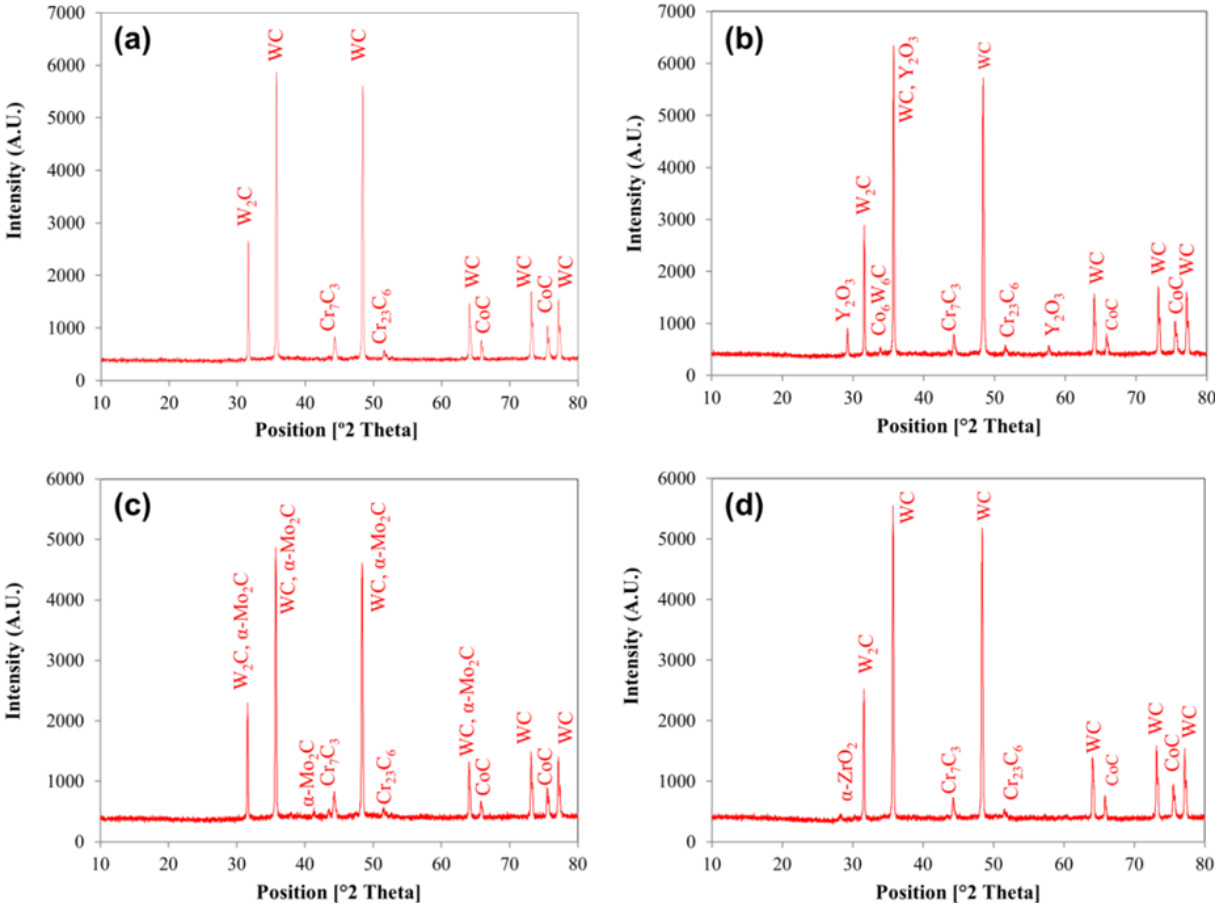

Fig. 4. XRD spectrums of (a) WOKA, (b) WOKA-Y, (c) WOKA-M, and (d) WOKA-Z coatings

3.4. Erosion Wear Analysis

3.4.1. Influence of Speed of Rotation

Slurry erosion of WOKA, WOKA-Y, WOKA-M, and WOKA-Z coatings at different rotational speeds for FA and BA particles is illustrated in Fig. 5(a) and 6(a) rotation [C= 30% (by wt.), T= 180 min, and α=0°]. In Fig. 5(a), it can be inferred that the slurry erosion is significantly influenced by the rotational speed of the tester. The speed of rotation of the propeller in a pot tester is directly related to the velocity of bulk FA particles. The speed of rotation of the propeller and the velocity of particles are associated with each other in the following manner:

$$V_{particles} \prec N_{propeller} \quad (1)$$

As per the above relationship, the particles' velocity increases with the speed of rotation of the propeller. Therefore, the conditions become accelerated at a high speed of rotation which is severe because the particles feel high kinetic energy at a high speed of rotation. High kinetic energy directs the particles toward the workpiece at high impact energy which is converted into the erosion action [43–47]. It was also seen that the WOKA-Y coating displays higher slurry erosion resistance than the standard WOKA, WOKA-M, and WOKA-Z coatings. The order of slurry erosion was established as WOKA-Y< WOKA-M< WOKA< WOKA-Z. A similar type of phenomenon and slurry erosion order was observed for the BA particles, as shown in Fig.

[DOI: 10.22068/ijmse.2834]

6(a) rotation [C= 30% (by wt.), T= 180 min, and α= 0°]. It was observed that the increment in slurry erosion with an increase in speed of rotation was lower in the case of FA particles as compared to BA particles. This happened because the BA particles are coarser than the FA particles. Moreover, the slurry erosion follows a non-linear characteristic with the speed of rotation.

3.4.2. *Influence of Time*

Fly ash (FA) slurry erosion results for the variation of testing time are illustrated in Fig. 5(b) [C= 60% (by wt.), α= 0°, and N= 1500 rpm]. It was observed that the increase in testing time causes higher slurry erosion experienced by various workpieces. The minimum slurry erosion was perceived WOKA-Y coating at 90 min of testing time. The results of the relative erosion wear by bottom ash slurry established by different time durations are represented in Fig. 6(b). By comparison of Fig. 5(b) and 6(b), it can be seen that FA slurry erosion wear was found to be more linear than BA slurry. This happened because the FA particles exhibit a spherical shape.

The shape of fly ash particles doesn't transform much with the time passage. It maintains a spherical shape even after the slurry erosion phenomenon. Although, the slurry erosion by BA particles showed a steeper increase in slurry erosion with testing time as compared to FA particles, as shown in Fig. 6(b).

3.4.3. *Influence of Concentration*

Fig. 5(c) and 6(c) illustrate the influence of concentration on slurry erosion of standard and modified WOKA cermet coatings by FA and BA particles, respectively. In Fig. 5(c), slurry erosion wear due to FA particles shows a steeper increase as the solid concentration increases. This occurs because the particles increase in the slurry as the higher concentration is used during experiments which directly contributes to the interaction phenomenon of slurry erosion. In other words, higher slurry concentration results in more collision of bulk particles to the workpiece; therefore, high erosion occurs (Gandhi et al. 2001; Desale et al. 2006).

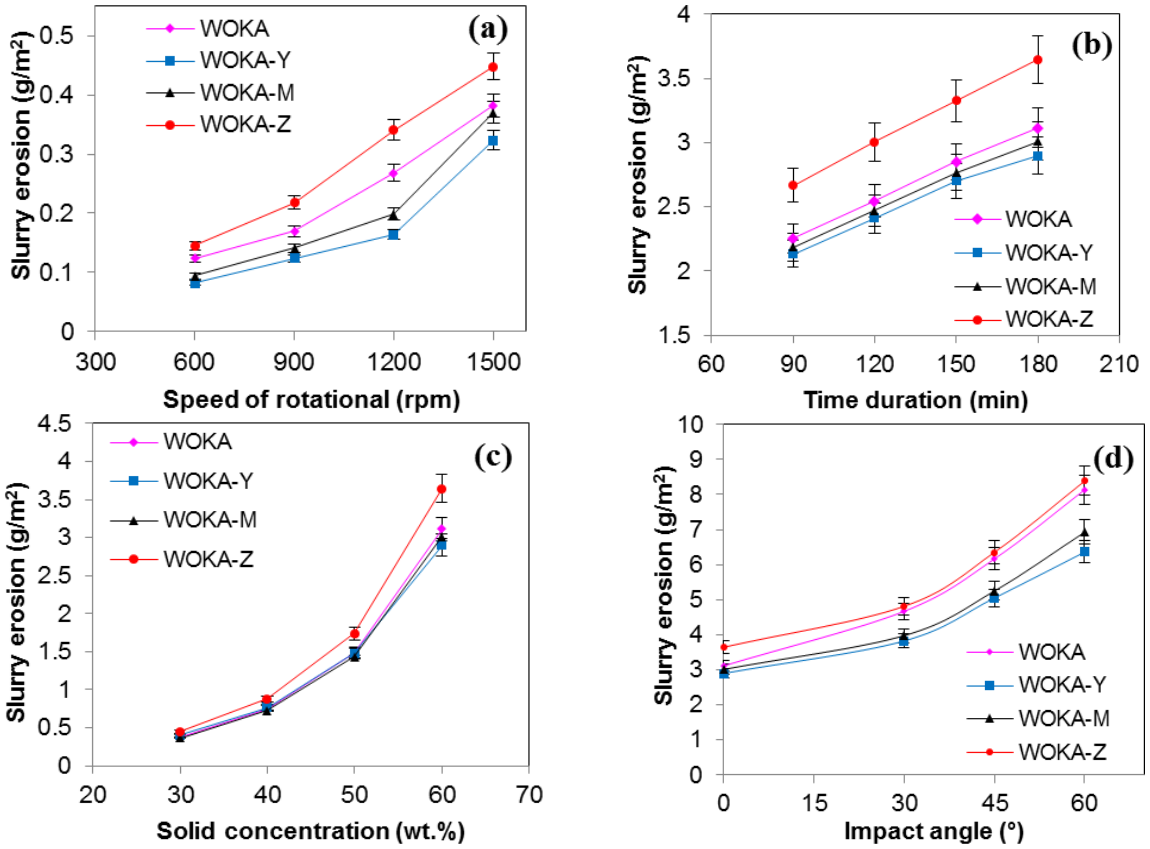

Fig. 5. Fly ash (FA) slurry erosion results for the variation of (a) speed of rotation rotation [*C*= 30% (by wt.), *T*= 90 min, and *α*=0°], (b) time [*C*= 60% (by wt.), *α*= 0°, and *N*= 1500 rpm], (c) concentration [*T*= 180 min, *α*= 0°, and *N*= 1500 rpm], and (d) impact angle [*T*= 180 min, *C*= 60% (by wt.), and *N*= 1500 rpm].

[DOI: 10.22068/ijmse.2834]

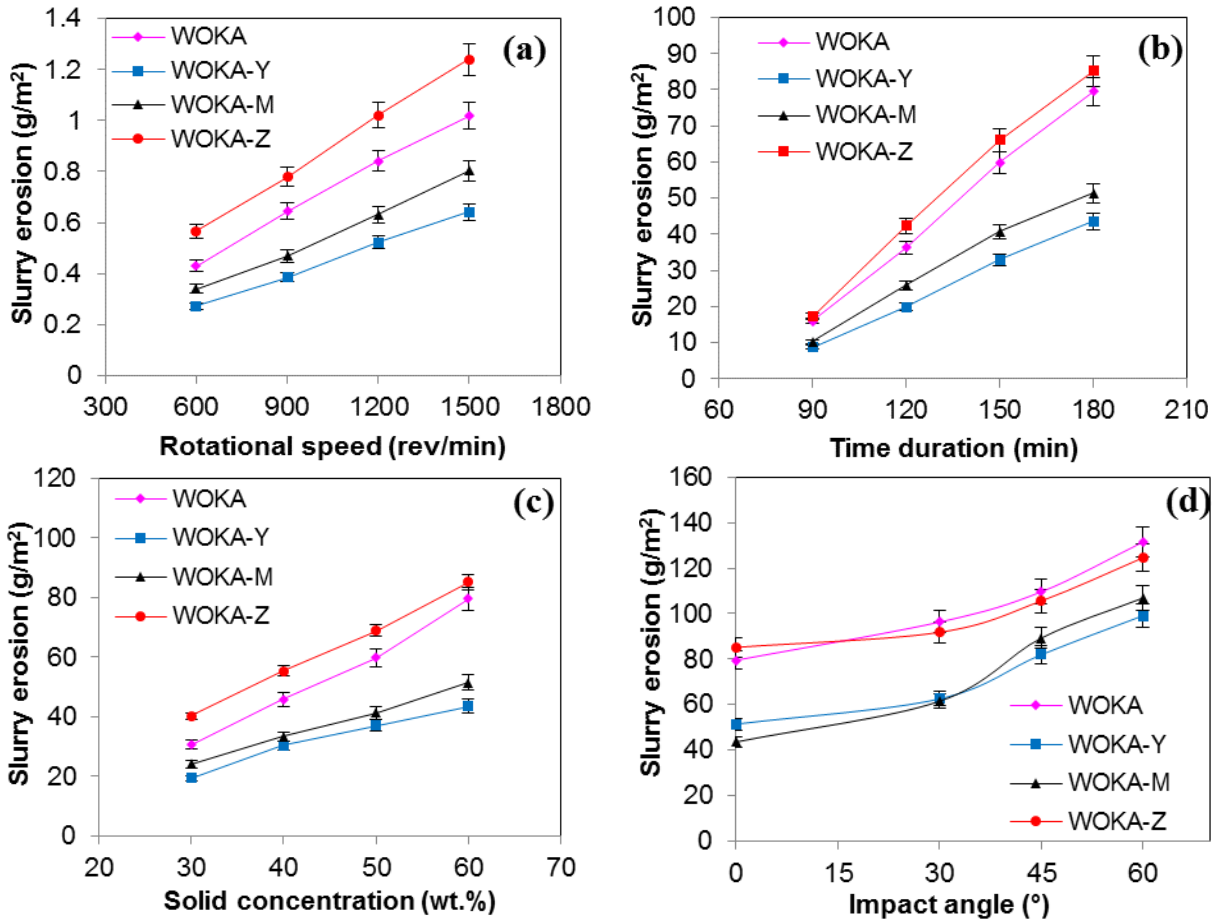

Fig. 6. Bottom ash (BA) slurry erosion results for the variation of (a) speed of rotation [C= 30% (by wt.), T= 180 min, and α= 0°], (b) time [C= 30% (by wt.), α= 0°, and N= 1500 rpm], (c) concentration [T= 180 min, α= 0°, and N= 1500 rpm], and (d) impact angle [T= 180 min, C= 60% (by wt.), and N= 1500 rpm].

In Fig. 5(c), it was also observed that the increment in erosion wear was almost the same for every 10% rise in the concentration of FA slurry. By comparison, it was demonstrated that the trend of slurry erosion by FA was different from erosion worn by BA slurry. FA particles flowing in slurry possess lower void spaces than the BA particles due to the increase in the concentration of fly ash resulting in a large number of particles in a given volume. Thus, the increment in FA slurry erosion for every 10% increase in concentration was high as compared to BA slurry.

In Fig. 6(c), it is seen that slurry erosion augments at a non-linear rate with an increase in concentration. At the initial increment (30-40%), the slurry erosion curve moves steeper. However, the steepness of the erosion curve drop to 40-50% concentration which further drops while the concentration increases from 50-60%. This type of finding is already reported in the literature for different materials and erodents [48, 49].

3.4.4. Influence of Impact Angle

Fig. 5(d) shows the effect of impact angle on FA slurry erosion of standard and modified WOKA powder coating. Maximum slurry erosion for FA slurry was perceived at a 60º impact angle for standard and modified WOKA coatings. The curve of slurry erosion specifies that standard and modified WOKA coatings show brittle characteristics. The sequence of FA slurry erosion for WOKA powder coatings is written as:

- WOKA-Y< WOKA-M< WOKA< WOKA-Z (at α= 0°, 30°, 45° and 60°).

The slurry erosion of WOKA coatings at different impact angles between BA particles and the workpiece is shown in Fig. 6(d). Different observations were made for the BA slurry. The order of BA slurry erosion for WOKA powder coatings is found as:

[DOI: 10.22068/ijmse.2834]

- WOKA-M< WOKA-Y< WOKA< WOKA-Z (at α= 0°).
- WOKA-M< WOKA-Y< WOKA-Z< WOKA (at α= 30°).
- WOKA-Y< WOKA-M< WOKA-Z< WOKA (at α= 45° and 60°).

3.5. Slurry Erosion Mechanisms

Slurry erosion wear relies on the material removal process, and the characteristics of the target material are responsible for the wear. To understand the material removal process, the analysis of microstructure plays a crucial role. In this context, the SEM technique was employed for the morphological analysis of eroded coatings. Researchers reported that the main type of slurry erosion that severely erode the material of centrifugal slurry pumps includes cutting, fracturing, and abrasion [43, 50].

In the present study, the erosion mechanisms of WOKA coatings were analyzed at T= 180 min, C= 60% (by wt.), α= 0°, and N= 1500 rpm. Fig. 7 shows the erosion mechanisms on WOKA coating by the effect of FA and BA slurry. In Fig. 7(a), wear marks can be observed on the worn WOKA coating's surfaces by the mechanical action of FA particles resulting from micro-cutting, smear, and delamination. It has also been discovered that the micro-crater wears the surface of the material, resulting in material loss. However, in the case of BA slurry; the craters and micro-cutting, were perceived on the surface of the WOKA coating, as illustrated in Fig. 7(b).

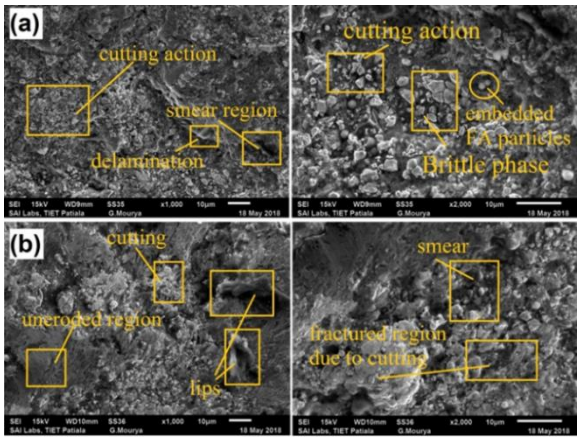

Fig. 7. Erosion mechanisms on WOKA coating by the effect of (a) FA and (b) BA slurry at T= 180 min, C= 60% (by wt.), α= 0°, and N= 1500 rpm

At higher magnification (×500), lip development appeared around the edge of the splats. The splats diminishing, however, appear to be more common in some areas. The micro-cutting action of the diminished splats also took place.

Erosion mechanisms of WOKA-Y coatings were analyzed at T= 180 min, C= 60% (by wt.), α= 0°, and N= 1500 rpm, as shown in Fig. 8. Fig. 8(a) presents the erosion mechanisms by the mechanical action of FA particles at the surface of WOKA-Y coating. Slurry erosion occurs at the surface of WOKA-Y coating was comparatively lower than standard WOKA coating. During the erosion, the splats remained undiminished in the case of FA slurry. Few pores can be also seen at higher magnification (×500). In Fig. 8(b), a few splats were detected at the surface of the WOKA-Y coating. Commonly observed mechanisms were smear regions, plowing, and craters.

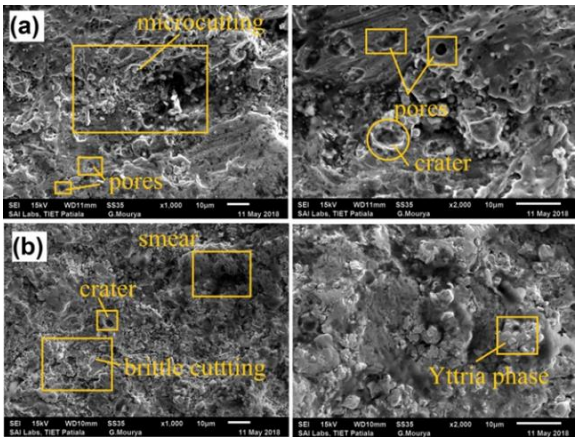

Fig. 8. Erosion mechanisms on WOKA-Y coating by the effect of (a) FA and (b) BA slurry at T= 180 min, C= 60% (by wt.), α= 0°, and N= 1500 rpm

Fig. 9(a) illustrated the worn surface of WOKA-M coatings by the FA particles. In Fig. 9(a), the craters and pores were seen frequently on the surface of the WOKA-M coating. The micro-cutting and plastic deformations appeared on the eroded surface. Melted splats also appeared in a few regions. WOKA-M coating shows the carters, plowing, and cutting action on the eroded surface, as seen in Fig. 9(b). Few micro hills were observed in the SEM micrographs. The particle tracks also appeared on the diminished surfaces of splats.

The erosion mechanism at the surface of WOKA-Z coating by FA particles is illustrated in Fig. 10(a). Dark regions i.e. craters appeared on the surface of WOKA-M coatings. The micro-

[DOI: 10.22068/ijmse.2834]

cutting, lip formation, and diminished splats are visualized on the eroded surface. WOKA-Z coating show splat delamination, deep craters, and plowing by erosion due to BA particles, as represented in Fig. 10(b). Zr-doped regions appeared which formed a flooded-sand-like microstructure which could be a constraint in the use of WOKA-Z coating. Zirconia addition in WOKA is recommended for corrosion problems.

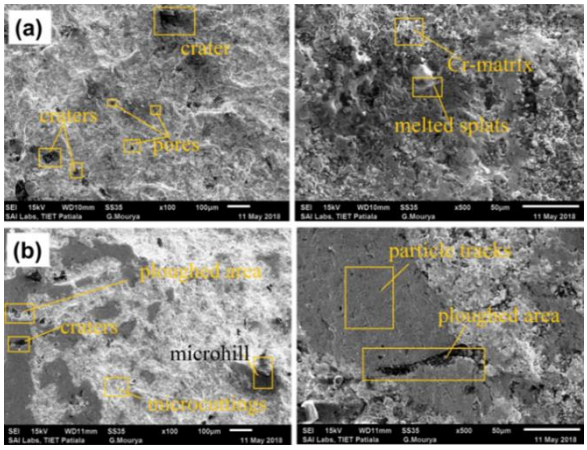

Fig. 9. Erosion mechanisms on WOKA-M coating by the effect of (a) FA and (b) BA slurry at T= 180 min, C= 60% (by wt.), α= 0°, and N= 1500 rpm

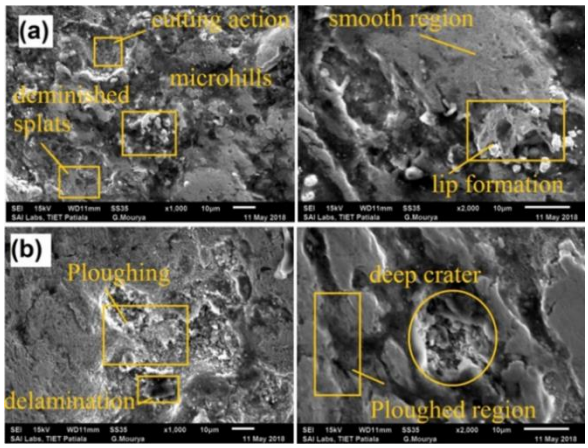

Fig. 10. Erosion mechanisms on WOKA-Z coating by the effect of (a) FA and (b) BA slurry at T= 180 min, C= 60% (by wt.), α= 0°, and N= 1500 rpm

4. CONCLUSIONS

The following conclusions are drawn based on experimental results:

- Microhardness of the WOKA was found as 1156± 27 H.V. Although, the microhardness of WOKA-Y, WOKA-M, and WOKA-Z coatings was measured as 1164±21, 1123±18, and 1089±32 H.V. respectively.
- The sequence of slurry erosion resistance of WOKA coatings for the variation of concentra-tion, time, and speed of rotation is found as WOKA-Y >WOKA-M >WOKA >WOKA-Z.
- The increment in slurry erosion was lower in the case of FA particles as compared to BA particles. This happened because the BA particles are coarser than the FA particles.
- Maximum slurry erosion for FA and BA slurry was perceived at a 60º impact angle for standard and modified WOKA coatings.
- The characteristic of slurry erosion specifies that standard and modified WOKA coatings show a brittle mode of failure.

ACKNOWLEDGEMENTS

Authors received no financial support from Institute/University or any funding agency or any non-profit/profit industry for the research, authorship, and/or publication of this article.

REFERENCES

[1] Altuncu, E., and Onen, B., "Solid particle erosive wear behaviour of flame sprayed EVA based polymeric coatings." J. Met. Mater. Miner., 2020, 30, 64–71.

[2] Singh, J., Kumar, S., and Mohapatra, S. K., "Erosion tribo-performance of HVOF deposited Stellite-6 and Colmonoy-88 micron layers on SS-316L." Tribol. Int., 2020, 147, 105262.

[3] Kamaraj, M., Project completion report: Life enhancement of hydro turbine components by surface coatings. New Delhi, India, 2008.

[4] Singh, J. Kumar, S., and Mohapatra, S. K., "Tribological performance of Yttrium (III) and Zirconium (IV) ceramics reinforced WC–10Co4Cr cermet powder HVOF thermally sprayed on X2CrNiMo-17-12-2 steel." Ceram. Int., 2019, 45, 17, 23126–23142.

[5] Singh, J., and Singh, J. P., "Numerical Analysis on Solid Particle Erosion in Elbow of a Slurry Conveying Circuit." J. Pipeline Syst. Eng. Pract., 2021, 12, 04020070.

[6] Singh, J., Singh, S., and Singh, J. P., "Investigation on wall thickness reduction of hydropower pipeline underwent to

[DOI: 10.22068/ijmse.2834]

erosion-corrosion process." Eng. Fail. Anal., 2021, 127, 105504.
[7] Prashar, G., and Vasudev, H., "Influence of heat treatment on surface properties of HVOF deposited WC and Ni-based powder coatings : a review," Surf. Topogr. Metrol. Prop., 2021, 9, 43002.
[8] Singh, P., Vasudev, H., and Bansal, A., "Effect of post-heat treatment on the microstructural, mechanical, and bioactivity behavior of the microwave-assisted alumina-reinforced hydroxyapatite cladding." Proc. IMechE Part E J Process Mech. Eng., 2022.
[9] Vasudev, H., Prashar, G., Thakur, L., and Bansal, A., "Microstructural characterization and electrochemical corrosion behaviour of HVOF sprayed Alloy718-nanoAl_2O_3 composite coatings." Surf. Topogr. Metrol. Prop., 2021, 9, 35003.
[10] Singh, G., Vasudev, H., and Bansal, A. "Influence of heat treatment on the microstructure and corrosion properties of the Inconel-625 clad deposited by microwave heating." Surf. Topogr. Metrol. Prop., 2021, 9, 025019.
[11] Vasudev, H., Thakur, L., Singh, H., and Bansal, A., "Erosion behaviour of HVOF sprayed Alloy718-nano Al_2O_3 composite coatings on grey cast iron at elevated temperature conditions." Surf. Topogr. Metrol. Prop., 2021, 9, 035022.
[12] Singh, G., Vasudev, H., Bansal, A., Vardhan, S., and Sharma, S. "Microwave cladding of Inconel-625 on mild steel substrate for corrosion protection," Mater. Res. Express, 2020, 7, 026512.
[13] Mohammed G. Basha, T., and Bolleddu, V., "Impact of carbon nanotubes reinforcement on microstructural and tribological characteristics of air plasma sprayed conventional alumina-titania (Al_2O_3- 3 wt% TiO_2) coatings." Iran. J. Mater. Sci. Eng., 2020, 17, 92–103.
[14] Buytoz, S., Ulutan, M., Islak, S., Kurt, B., and Çelik, O. "Microstructural and Wear Characteristics of High Velocity Oxygen Fuel (HVOF) Sprayed NiCrBSi-SiC Composite Coating on SAE 1030 Steel." Arab. J. Sci. Eng., 2013, 38, 1481–1491.
[15] Vasudev, H., Thakur, L., Bansal, A., Singh, H., and Zafar, S., "High Temperature Oxidation and Erosion Behaviour of HVOF Sprayed Bi-Layer Alloy-718/NiCrAlY Coating," Surf. Coatings Technol., 2019, 362, 366–380.
[16] Vasudev, H., Prashar, G., Thakur, L., and Bansal, A., "Electrochemical corrosion behavior and microstructural characterization of HVOF sprayed Inconel718-Al_2O_3 composite coatings," Surf. Rev. Lett., 2022, 29(2), p. 2250017.
[17] Vasudev, H., Thakur, L., Singh, H., and Bansal, A., "Effect of Addition of Al2O3 on the High-Temperature Solid Particle Erosion Behaviour of HVOF Sprayed Inconel-718 Coatings," Mater. Today Commun., 2022, 30, 103017.
[18] Vasudev, H., Thakur, L., Singh, H., and Bansal, A., "A Study on Processing and Hot Corrosion Behaviour of HVOF sprayed Inconel718-Nano Al_2O_3 Coatings," Mater. Today Commun., 2020, 25, 101626.
[19] Vasudev, H., Prashar, G., Thakur, L., and Bansal, A., "Electrochemical Corrosion Behavior and Microstructural Characterization of HVOF Sprayed Inconel-718 Coating on Gray Cast Iron," J. Fail. Anal. Prev., 2020, 21, 250–260.
[20] Vasudev, H., Singh, P., Thakur, L., and Bansal, A., "Mechanical and Microstructural Characterization of Microwave Post Processed Alloy-718 Coating," Mater. Res. Express, 2019, 6, 1265f5.
[21] Vasudev, H., Thakur, L., Singh, H., and Bansal, A., "An Investigation on Oxidation Behaviour of High Velocity Oxy-Fuel Sprayed Inconel718-Al_2O_3 Composite Coatings," Surf. Coatings Technol., 2020, 393, 125770.
[22] Prashar, G., and Vasudev, H., "Parameters and Heat Treatment on the Corrosion Performance of Ni-Based Thermal Spray Coatings," Surf. Rev. Lett., 2022, 29, 1–18.
[23] Prashar, G., Vasudev, H., and Thakur, L., "High-Temperature Oxidation and Erosion Resistance of Ni-Based Thermally-Sprayed Coatings used in Power Generation Machinery : A Review," Surf. Rev. Lett., 2022, 29, 2230003.
[24] Prashar, G., and Vasudev, H., "Structure-

[DOI: 10.22068/ijmse.2834]

Property Correlation and High-Temperature Erosion Performance of Inconel625-Al_2O_3 Plasma-Sprayed Bimodal Composite Coatings," Surf. Coatings Technol., 2022, 439, 128450.

[25] Vasudev, H., "Wear Characteristics of Ni-WC Powder Deposited by Using a Microwave Route on Mild Steel: Microwave Cladding of Ni-WC," Int. J. Surf. Eng. Interdiscip. Mater. Sci., 2020, 8, 44–54.

[26] Szala, M., Hejwowski, T. J., and Lenart, I., "Cavitation erosion resistance of Ni-Co based coatings." Adv. Sci. Technol. Res. J., 2014, 8, 36–42.

[27] Szala, M., Łatka, L., Walczak, M., and Winnicki, M. "Comparative Study on the Cavitation Erosion and Sliding Wear of Cold-Sprayed Al/Al_2O_3 and Cu/Al_2O_3 Coatings, and Stainless Steel, Aluminium Alloy, Copper and Brass." Metal., 2020, 10, 1–24.

[28] Hussain, A. K., and Al Naib, U. M. B., "Recent developments in graphene based metal matrix composite coatings for corrosion protection application: A review." J. Met. Mater. Miner., 2019, 29, 1–9.

[29] Singh, J., "Slurry erosion performance analysis and characterization of high-velocity oxy-fuel sprayed Ni and Co hardsurfacing alloy coatings." J. King Saud Univ. - Eng. Sci., 2021 (in press).

[30] Vadapalli, S., Pathem, U., Vuppala, V., Chebattina, K. R., and Sagari, J., "Corrosion and cavitation erosion properties of sub-micron WC-Co/Cr_3C_2-NiCr multi-layered coating on aluminium substrates." J. Met. Mater. Miner., 2020, 30, 46–54.

[31] Farzan, F., Shahverdi, H. R., and Ghaeni, F. M., "Effect of wet and dry conditions on wear behavior of amorphous coating of Fe-Cr-Mo-Nb-C-B." Iran. J. Mater. Sci. Eng., 2018, 15, 76–87.

[32] Wheeler, D. W., and Wood, R. J. K., "Erosion of hard surface coatings for use in offshore gate valves." Wear, 2005, 258, 526–536.

[33] Maiti, A. K., Mukhopadhyay, N., and Raman, R., "Effect of adding WC powder to the feedstock of WC-Co-Cr based HVOF coating and its impact on erosion and abrasion resistance." Surf. Coatings Technol., 2007, 201, 7781–7788.

[34] Lee, C. W., Han, J. H., Yoon, J., Shin, M. C., and Kwun, S. I., "A study on powder mixing for high fracture toughness and wear resistance of WC-Co-Cr coatings sprayed by HVOF," Surf. Coatings Technol., 2010, 204, 2223–2229.

[35] Cho, T. Y., Yoon, J. H., Kim, K. S., Song, K. O., Joo, Y. K., Fang, W., Zhang, S. H., Youn, S. J., Chun, H. G., and Hwang, S. Y., "A study on HVOF coatings of micron and nano WC-Co powders." Surf. Coatings Technol., 2008, 202, 5556–5559.

[36] Thakur, L., Arora, N., Jayaganthan, R., and Sood, R., "An investigation on erosion behavior of HVOF sprayed WC-CoCr coatings." Appl. Surf. Sci., 2011, 258, 1225–1234.

[37] Vite-Torres, M., Laguna-Camacho, J. R., Baldenebro-Castillo, R. E., Gallardo-Hernández, E. A., Vera-Cárdenas, E. E., and Vite-Torres, J., "Study of solid particle erosion on AISI 420 stainless steel using angular silicon carbide and steel round grit particles." Wear, 2013, 301, 383–389.

[38] Singh, J., Kumar, S., and Mohapatra, S. K., "An erosion and corrosion study on thermally sprayed WC-Co-Cr powder synergized with $Mo_2C/Y_2O_3/ZrO_2$ feedstock powders," Wear, 2019, 438–439, 102751.

[39] ASTM-G76-95, Standard test method for conducting erosion tests by solid particle impingement using gas jets. ASTM International, USA, 2000.

[40] Yang, K., Zhou, X., Zhao, H., and Tao, S., "Microstructure and mechanical properties of Al_2O_3-Cr_2O_3 composite coatings produced by atmospheric plasma spraying." Surf. Coatings Technol., 2011, 206, 1362–1371.

[41] Singh, J., and Singh, S., "Neural network supported study on erosive wear performance analysis of Y_2O_3/WC-10Co4Cr HVOF coating." J. King Saud Univ. - Eng. Sci., 2022 (in press).

[42] Singh, J., and Singh, J. P., "Performance analysis of erosion resistant Mo_2C reinforced WC-CoCr coating for pump impeller with Taguchi's method." Ind.

[DOI: 10.22068/ijmse.2834]

Lubr. Tribol., 2022, 74, 431–441.
[43] Gandhi, B. K., Singh, S. N., and Seshadri, V. “Study of the parametric dependence of erosion wear for the parallel flow of solid-liquid mixtures.” Tribol. Int., 1999, 32, 275–282.
[44] Tarodiya, R., and Gandhi, B. K., “Experimental Investigation on Slurry Erosion Behavior of 304L Steel, Grey Cast Iron, and High Chromium White Cast Iron.” J. Tribol., 2019, 141, 1–11.
[45] Desale, G. R., Gandhi, B. K., and Jain, S. C., “Improvement in the design of a pot tester to simulate erosion wear due to solid-liquid mixture.” Wear, 2005, 259, 196–202.
[46] Desale, G. R., Gandhi, B. K., and Jain, S. C., “Effect of erodent properties on erosion wear of ductile type materials.” Wear, 2006, 261, 914–921.
[47] Desale, G. R., Gandhi, B. K., and Jain, S. C., “Development of correlations for predicting the slurry erosion of ductile materials.” J. Tribol., 2011, 133, 1–10.
[48] Singh, J., “Wear performance analysis and characterization of HVOF deposited Ni–20Cr_2O_3, Ni–30Al_2O_3, and Al_2O_3–13TiO_2 coatings.” Appl. Surf. Sci. Adv., 2021, 6, 100161.
[49] Singh, J., “A review on mechanisms and testing of wear in slurry pumps, pipeline circuits and hydraulic turbines.” J. Tribol., 2021, 143, 090801.
[50] Gandhi, B. K., Singh, S. N., and Seshadri, V., “A study on the effect of surface orientation on erosion wear of flat specimens moving in a solid-liquid suspension.” Wear, 2003, 254, 1233–1238.

[DOI: 10.22068/ijmse.2834]